Congenital and Acquired Heart Disease

S. Ley, B.K. Han, R. Arnold, and J.R. Lesser

Abstract

CT has been introduced cautiously in the pediatric and young adult cardiac patient population due to concerns about radiation. Advances in CT technology have resulted in improved spatial and temporal resolution, providing excellent image quality even in neonates with high heart rates. Radiation dose reduction techniques and rapid image acquisition techniques that limit anesthesia needs have decreased the risk of CT for children. CT is an excellent modality for specific congenital cardiac indications when information is needed to supplement echocardiographic findings and when MRI is contraindicated or considered high risk.

23.1 Introduction

Congenital heart disease (CHD) is the most common congenital anomaly. The spectrum of CHD malformations ranges from relatively simple lesions, which are hemodynamically insignificant, to very complex lesions requiring multiple interventions and lifelong surveillance. About two to three out of 1,000 newborns are born with complex congenital heart disease. A majority of patients with even the most complex anomalies are expected to survive to adulthood. There are now more adults with palliated CHD than those followed in the traditional pediatric age range.

Echocardiography remains the most widely used diagnostic modality for patients with CHD, and when additional information is needed, magnetic resonance imaging (MRI) is the procedure most commonly performed. Cardiac CT is primarily used when there are

M. Dewey, *Cardiac CT*,
DOI 10.1007/978-3-642-41883-9_26, © Springer-Verlag Berlin Heidelberg 2014

contraindications to MRI or imaging artifacts degrade diagnostic quality.

CT angiography (CTA) in CHD patients is most commonly indicated for evaluation of arterial and venous anomalies in newborns and for postoperative evaluation of complex disease in older children and adults with contraindications to MRI. This chapter focuses on the most frequent CHD diagnoses referred for CTA and the lesions most commonly found on studies ordered for different indications.

23.2 Technical Considerations

All aspects of CT in the CHD population must be tailored to the size of the patient and the referral indication for imaging. Well-trained CT technicians and direct physician oversight of the exam are required for the complex CHD population due to the variability of patient anatomy and physiology.

23.2.1 Size of Vascular Structures

The submillimeter isotropic resolution of today's CT scanners provides excellent visualization of even small vessels. As children get older, the diameters of all structures increase in size proportionate to growth (**Table 23.1**). Pediatric cardiac structures are often indexed to body surface area from infancy through adolescence. When no CT-specific data are available for indexing a structure to body surface area, echocardiography-based standard deviations (z-score) may be used. A z-score is the number of standard deviations from the 50th percentile for a cardiac structure based on a normal distribution. Thus, a positive standard score represents a deviation above the mean, while a negative standard score represents a deviation below the mean.

23.2.2 Heart Rate and Premedication for Coronary Artery Imaging

The resting heart rates of infants, children, and adolescents are higher than those of adults, and there is more heart rate variability with respiratory changes (sinus arrhythmia, **Table 23.2**). The image acquisition window of current-generation CT scanners is as low as 75 ms, allowing coronary imaging even at higher heart rates. Coronary artery imaging is recommended in pediatric patients for evaluation of potentially malignant coronary artery anomalies, after surgical manipulation or reimplantation, and for evaluation of stenosis or coronary pathology in patients with a history of Kawasaki disease, systemic inflammatory disease, or Williams Beuren syndrome (aortic or pulmonary artery stenosis).

Beta blockade and other medication protocols have been used safely in healthy children to decrease the heart rate and improve the quality of coronary imaging. For patients with chronic heart failure or in those who are critically ill, beta blockade may be clinically

Table 23.1 Age-related diameters and growth rate of great arteries in children

Vessel	Day 1 (mean weight: 2.2 kg)	Three years (mean weight: 20 kg)	Weight-adapted growth per kg weight gain
Ascending aorta (mm)	8.4	14	0.43
Aortic arch (mm)	6.8	14.4	NA
Aortic isthmus (mm)	4.7	8.3	NA
Main pulmonary artery (mm)	7.5	14	0.5
Right pulmonary artery (mm)	4.3	8.6	0.33
Left pulmonary artery (mm)	4.2	8.8	0.35

Data were obtained in 130 normal newborns and infants by Trowitzsch et al.; diameters were measured by echocardiography. Linear growth of the great arteries within the first 3 years of life was found
NA not available

Table 23.2 Age-related heart rates in children

Age (years)	Heart rate (beats per min)
<1	110–160
1–2	100–150
2–5	95–140
5–12	80–120
>12	60–100

contraindicated (Chap. 6). The use of premedication must be tailored to individual patients and their current clinical status.

23.2.3 Respiratory and Motion Artifacts

The newest-generation volumetric or high-pitch scanners can acquire the scan range of a pediatric thorax in one heart beat, or a fraction of a second, which has reduced anesthesia and intubation needs in young patients. Many scans can be performed during free breathing without loss of image quality due to motion artifacts. For some older-generation scanners with image acquisition over several seconds, intubation or sedation may be required to obtain a scan without respiratory motion artifacts. The use of anesthesia and sedation will be dependent on the scanner available at each institution and the amount of detail required from the CT scan.

23.2.4 Intravenous Access and Contrast Agent Injection

Many types of peripheral access can be used for cardiac CT scans in patients with congenital anomalies including peripherally inserted central catheter (PICC) lines, umbilical venous lines, peripheral intravenous (IV) lines, and central venous lines. In the presence of intracardiac shunting, elimination of air bubbles in the injection is particularly important to avoid potential arterial emboli. Low flow rates are recommended when using a 24- or 22-gauge IV access. Careful observation of the IV site during a saline injection is recommended to confirm patency before the contrast agent is injected. Safe power injection through 24–18 gauge IV lines has been reported in pediatric patients. The contrast injection rate through a 24-gauge IV line is typically 0.5–1.0 ml/s and up to 1.5–2 ml/s through a 22-gauge IV access (**Table 23.3**).

23.2.5 IV Line Placement and Injection Protocols

The total contrast agent volume used for pediatric CT angiography is typically 1–2 ml/kg. For pulmonary or arterial angiography without intracardiac mixing, the IV line may be placed in any extremity and an automatic trigger used for image acquisition. A biphasic injection protocol can be used for simultaneous opacification of right- and left-sided cardiac structures.

Table 23.3 Recommended contrast agent injection protocols in children

Age (years)	Preparation
<1	24–22 G venous line as proximal as possible
	0.5–1.0 ml/s for 24 G (<100 psi)
	1–1.5 ml/s for 22 G
	1–2 ml/kg total contrast volume
1–2	22 G venous line as proximal as possible
	1–2 ml/s, psi < 150
	1–2 ml/kg total contrast volume
>2–5	22 G venous line
	2 ml/s
	1–2 ml/kg total contrast volume
>5	18–20 G venous line
	2–5 ml/s
	1–2 ml/kg total contrast volume

23.2.6 Scanning Protocol

Every pediatric CT scan must be adjusted to deliver the lowest radiation dose to obtain a diagnostic image according to the "as low as reasonably achievable" (ALARA) principle. Familiarity with the doses delivered with different scan modes is necessary and allows choosing the scan mode with the least risk for each specific indication. CT scanner output should be adjusted to the patient's size. Using dose reduction techniques allows mSv or sub-mSv imaging for many pediatric indications, including coronary artery imaging.

For anatomic scans, high-pitch or the volumetric scan mode may be used on latest-generation scanners. On older-generation scanners, anatomic scanning is most commonly performed without ECG triggering.

Coronary artery and functional imaging require ECG triggering on all scanner platforms. Several different scan modes are available for coronary artery imaging. The lowest dose technique deemed adequate for the individual patient's heart rate should be used.

For pediatric cardiovascular CT, no general recommendation for kV and mAs settings can be provided. For dose comparison, the dose length product (DLP) should

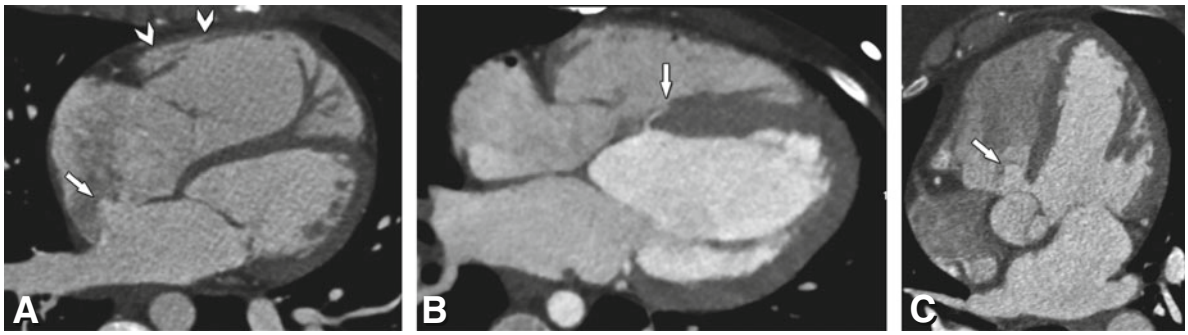

Fig. 23.1 Atrial and ventricular septal wall defects in three patients. **Panel A** shows a centrally located secundum atrial septal defect with contrast shunting from the left to right atrium (*arrow*). Note the right ventricular enlargement in this patient (*arrowheads*). The patient underwent successful device closure of the defect. **Panel B** shows a tiny basal muscular ventricular septal defect (*arrow*). This defect is located just inferior to the perimembranous area; most defects will be located more apically. Note that there was no relevant contrast jet from the left to the right ventricle and the lesion was considered hemodynamically insignificant. **Panel C** shows a large perimembranous ventricular defect located adjacent to the tricuspid valve just inferior to the aortic valve. Note the resulting positive contrast jet from the left to right ventricle in this patient (*arrow*)

be used. In our experience, a DLP as low as 4–8 mGy*cm (70 or 80 kV) is sufficient for imaging a baby weighing 3–4 kg. Only a minor increase in DLP is necessary with increasing weight, as the thoracic diameter stays rather constant during the first years of life. The most common indication for CT angiography in the neonatal CHD population is for evaluation of aortic or pulmonary artery pathology or for characterization of complex systemic and pulmonary venous anomalies prior to intervention. Many postoperative patients will have metallic implants and devices that degrade image quality of MRI. CT is also valuable for coronary artery assessment in patients with a history of Kawasaki disease aneurysm and for assessment of bileaflet mechanical valve function.

23.3 Atrial and Ventricular Septal Defects

The most common congenital anomalies are atrial (7%) and ventricular septal (31%) wall defects (**Fig. 23.1**). However, the role of CT in patients who are referred for preoperative evaluation of ventricular or atrial septal wall defects is limited. Echocardiography and MRI are the main diagnostic modalities for these lesions.

List 23.1. Aortic anomalies and defects

1. Persistent ductus arteriosus (PDA, **Fig. 23.3**)
2. Anomalies of the ascending aorta and of the aortic arch
   - (a) Hypoplastic arch (**Fig. 23.3**)
   - (b) Aortic rings
     - (i) Double aortic arch
     - (ii) Right-sided aortic arch with aberrant left subclavian artery and left-sided ductus arteriosus
     - (iii) Left-sided aortic arch with Lusoria artery
   - (c) Interrupted aortic arch
   - (d) Truncus arteriosus
3. Aortic stenosis and coarctation
   - (a) Coarctation (**Figs. 23.3** and **23.4**)
   - (b) Other aortic stenosis, e.g., subvalvular
4. Rare anomalies, e.g., aneurysm of the ductus arteriosus
5. Complications after interventions and/or surgery (**Fig. 23.4**)
6. Marfan syndrome (development of aortic root dilatation)
7. Ulrich-Turner syndrome (associated with aortic coarctation)

23.4 Aortic Arch

Congenital anomalies of the aorta are one of the most frequent cardiovascular malformations. They include a wide spectrum of diseases (**List 23.1**) ranging from patent ductus arteriosus (**Fig. 23.2**, 5–10% of all CHD) to aortic coarctation (8–10%, **Fig. 23.3**). The initial diagnosis is usually established by echocardiography. Blood pressure difference between the upper and lower extremity

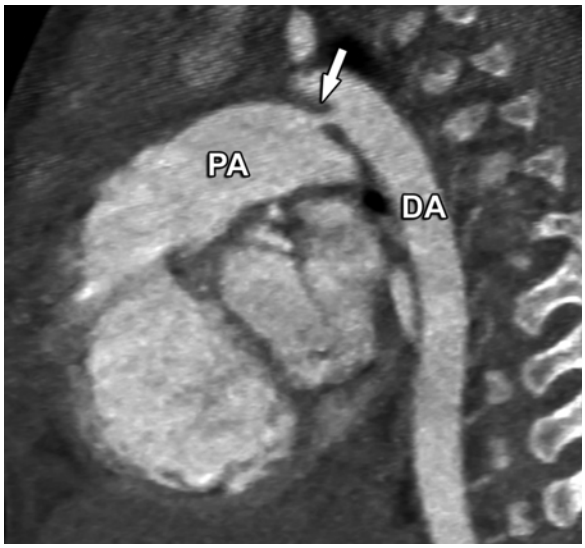

Fig. 23.2 Tiny ductus arteriosus (*arrow*) between the proximal descending aorta (*DA*) and the distal pulmonary artery (*PA*). This was an incidental finding on a CT performed for evaluation of the coronary arteries

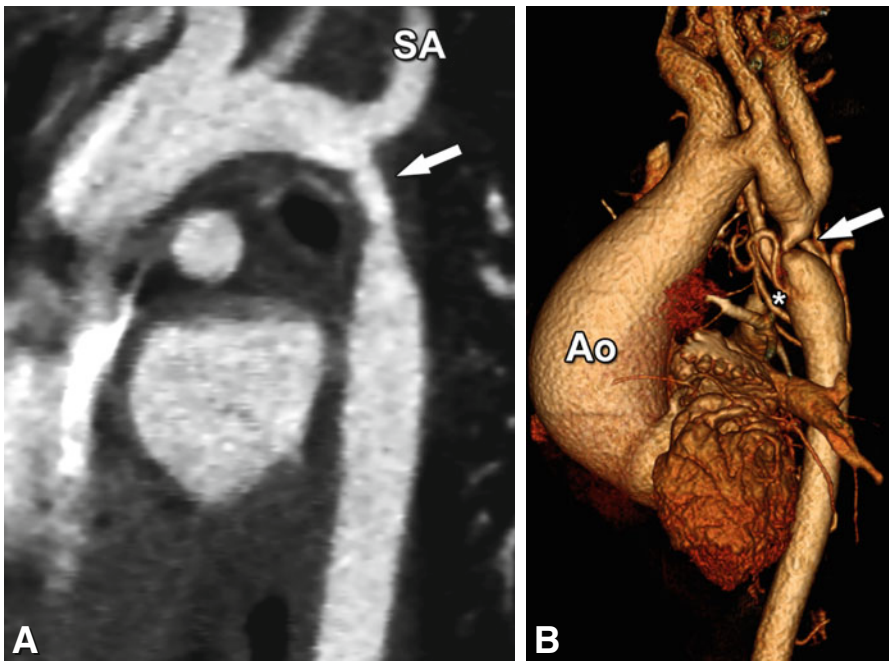

Fig. 23.3 Aortic coarctation in two patients. **Panel A** is a double-oblique image from a prospectively ECG-triggered CT scan showing coarctation in a 2-year-old patient (*arrow*) just distal to the takeoff of the left subclavian artery (*SA*). The high-pitch CT scan was performed during free breathing with an acquisition time of 0.25 s and a dose-length product of 6 Gy.cm. The patient underwent subsequent repair of coarctation with an end-to end anastomosis. **Panel B** shows a three-dimensional reconstruction of a CT scan performed for evaluation of severe aortic coarctation (*arrow*) in an 11-year-old patient who presented for evaluation of a murmur. His ascending aorta (*Ao*) was dilated and the murmur was secondary to aortic insufficiency. He was noted to be hypertensive with a blood pressure gradient of 30 mmHg between the right arm and leg. Note the collateral vessels supplying the descending aorta (*asterisk*). He underwent surgical repair of aortic coarctation and has since been followed clinically for aortic insufficiency and aortic root dilation

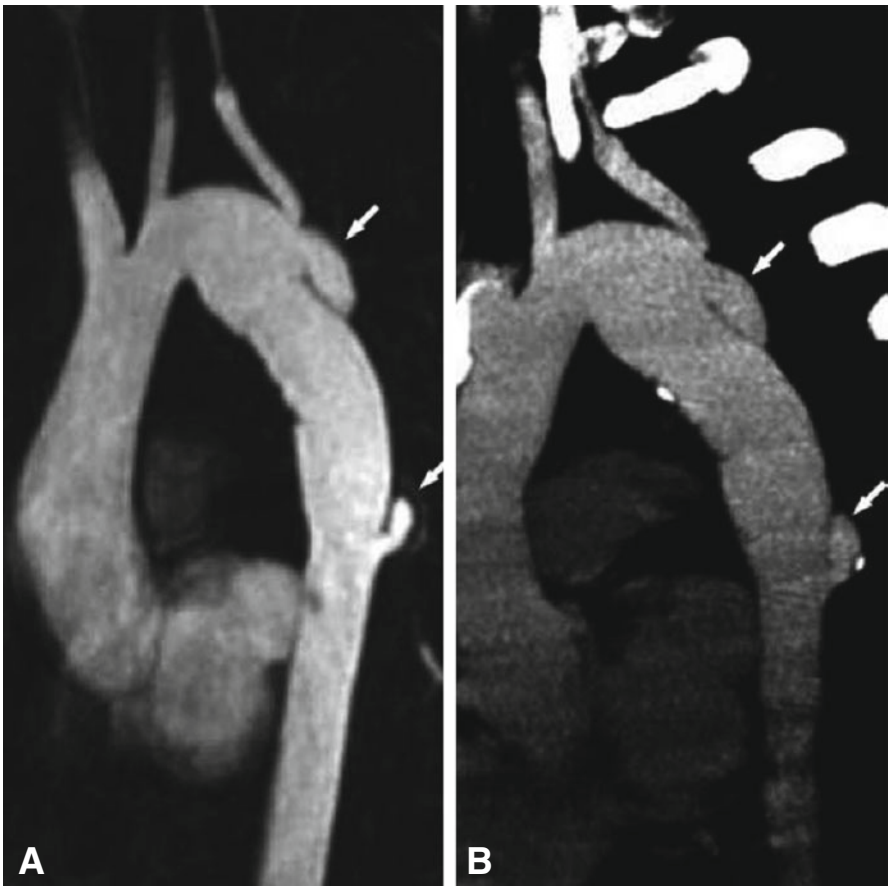

Fig. 23.4 Dissection as a complication after aortic arch operation in a 24-year-old female patient with congenital hypoplasia of the distal aortic arch and patch angioplasty at the age of 2 years. Eight years later a restenosis was diagnosed and a vascular prosthesis (16-mm Hemashield) was implanted. Regular follow-up was performed by MRI. **Panel A** is an MR angiography after intravenous contrast agent administration (10-mm double-oblique maximum intensity projection) that shows new dissections at the proximal and distal anastomosis of the prosthesis (*arrows*). For further surgical planning a nongated CT was performed (**Panel B**, 5-mm maximum intensity projection), which confirmed the MRI findings

is used to determine the pressure gradient unless there is an aberrant subclavian artery that does not allow a pre-coarctation pressure estimate. Doppler echocardiography is helpful in these cases, and catheterization is rarely required prior to surgical intervention for aortic coarctation at most centers. Noncritical stenosis or critical stenosis with well-developed collateral flow to the descending aorta is often detected in grown-ups who present with arterial hypertension and have blood pressure differences between arms and legs. Clinical indications for follow-up examinations are re-coarctation (<3%, higher when operated on in infancy) and postoperative aneurysms (24% after patch angioplasty) or dissection (5–50% after patch angioplasty, **Fig. 23.4**). Because it lacks radiation exposure and allows functional assessment (e.g., flow quantification), MRI is the preferred test in suspected coarctation (**Fig. 23.5**). As patients grow older, MRI may gain an increasing role as the acoustic window for echocardiography becomes poorer with age. CT has an indication in the follow-up of patients with coarctation who have stents, as the intraluminal visualization of stents is excellent (**Fig. 23.6**). In complex aortic arch abnormalities (i.e., double aortic arch), surgeons prefer to have a three-dimensional display of the

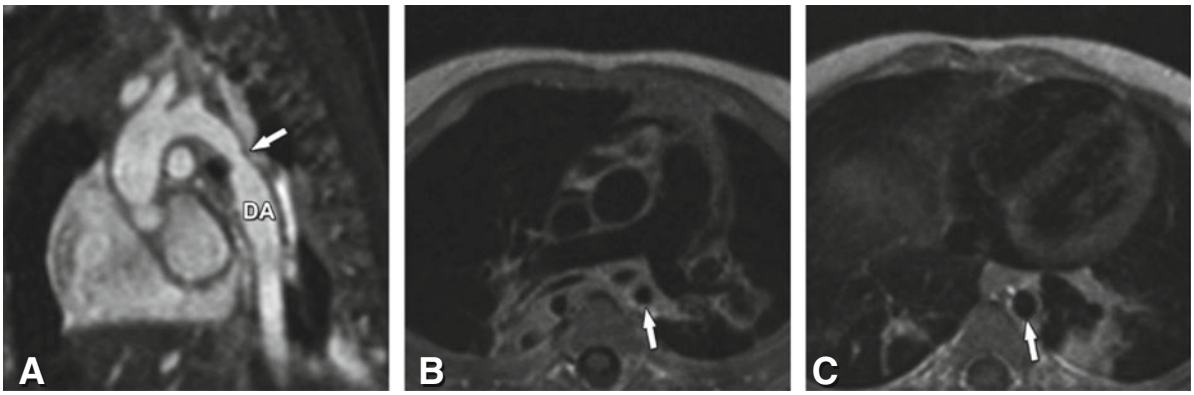

Fig. 23.5 Coarctation of the aorta in a 5-month-old male baby. **Panel A** is an ECG- and respiratory-gated steady-state free precession three-dimensional sequence (MR angiography) without contrast agent administration and demonstrates focal narrowing (*arrow*) of the descending aorta (*DA*). **Panel B** is a spin-echo MRI sequence with dark-blood pulse preparation, which shows the narrowing of the aorta in axial orientation (*arrow*), while **Panel C** shows the normal lumen of the descending aorta (*arrow*) on the same sequence at the level of the diaphragm. Note that the consolidation in the left lower lung seen on **Panel C** is due to a prior pneumonia in this patient

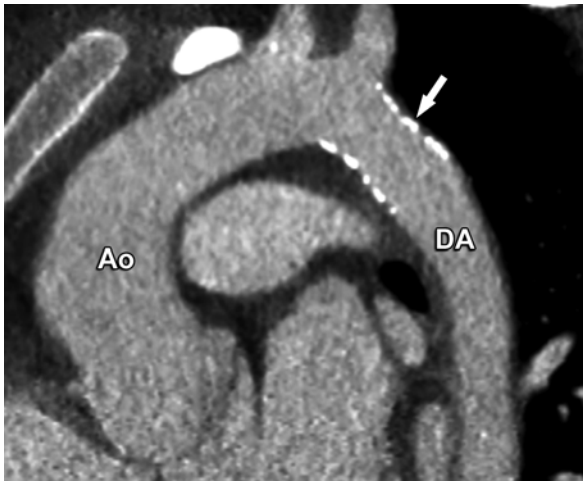

Fig. 23.6 Follow-up CT in an 18-year-old patient after interventions for aortic coarctation. The patient underwent left subclavian flap repair of aortic coarctation as an infant and later required balloon angioplasty of recurrent coarctation with stent placement (*arrow*). The CT was performed with prospective ECG triggering using 80 kV and a scan range limited to the area of interest. Note the absence of a left subclavian artery from the transverse aortic arch due to the initial repair and excellent visualization of the stent and aortic wall. *Ao* aorta, *DA* descending aorta

anatomic relationship between the trachea and the vascular structures. This information can be nicely provided by CT, even in critically ill children. A potential vascular ring associated with a right aortic arch, an aberrant left subclavian artery, and a left-sided ductal ligamentum are common and may be detected incidentally or cause pulmonary pathology. Evaluation of the airways relative to the vessels can be crucial in determining the clinical significance of the finding.

23.4.1 Persistent Ductus Arteriosus

During fetal life the ductus arteriosus connects the main pulmonary artery near its bifurcation to the aorta just beyond the origin of the left subclavian artery. The ductus arteriosus usually closes functionally soon after birth through muscular contractions. A persistent ductus arteriosus (PDA) is encountered in approximately 7% of all congenital heart defects. Echocardiography is the modality of choice for assessment of the ductus arteriosus in infants. CT is only performed if a complex malformation is suspected (**Figs.** 23.2 and 23.7).

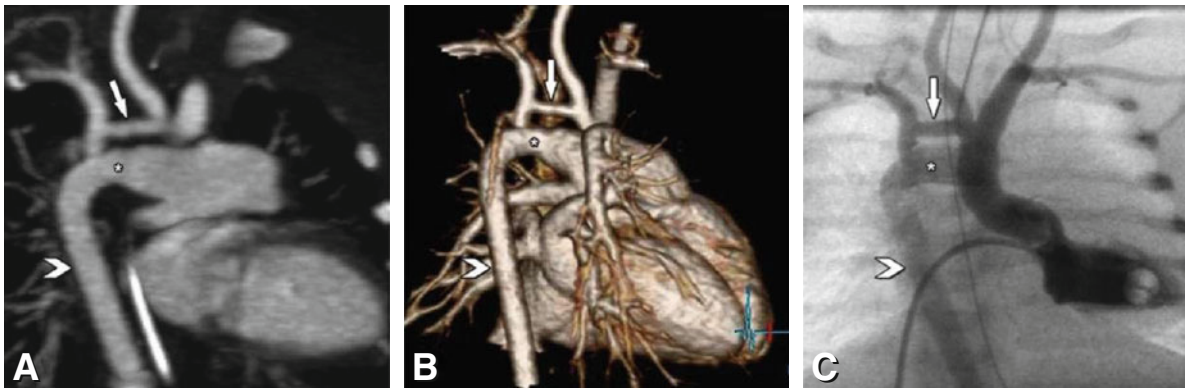

Fig. 23.7 Hypoplastic aortic arch (*arrow*) and large persistent ductus arteriosus Botalli (*asterisk*) in a 2-day-old child prenatally diagnosed with a cardiac malformation. On a double oblique maximum intensity projection (**Panel A**) the large persistent ductus arteriosus and the hypoplastic aortic arch (*arrow*) are shown. The persistent ductus arteriosus connects the main pulmonary artery and the descending aorta (*arrowhead*), which is normal. For operative planning the CT images were additionally presented to the surgeon as three-dimensional volume renderings (**Panel B**). **Panel C** presents the corresponding image from left ventricular catheterization

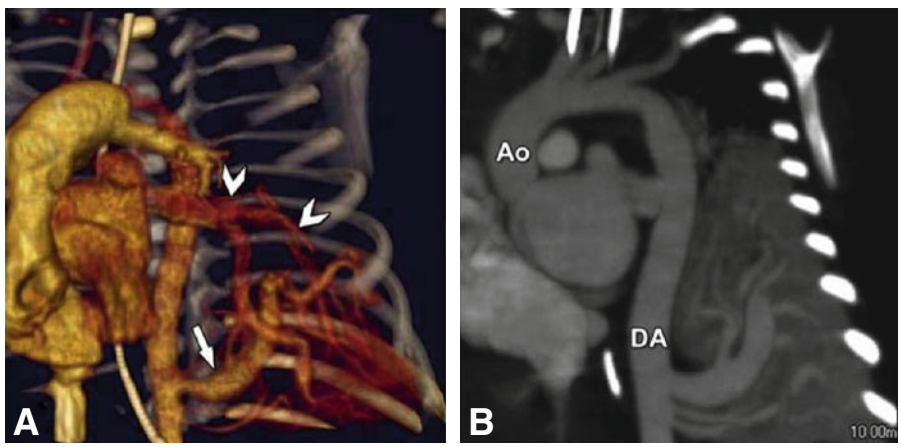

Fig. 23.8 Lung sequestration in a 15-day-old female baby with a prenatally diagnosed anomaly of the left lung. ECG-gated CT was performed using 7 ml contrast agent with 250 mg I/ml at an injection rate of 0.3 ml/s. **Panel A** shows a volume rendering of the arterial supply (three vessels) of the sequestration from the descending aorta (*arrow*). Venous drainage is to the left atrium (*arrowheads*). **Panel B** is a double-oblique maximum intensity projection along the ascending aorta (*Ao*) and descending aorta (*DA*) showing the three arteries supplying the sequestration from the *DA*. Due to the large size of the arterial supply the patient went to surgery for clipping of the arteries

23.4.2 Sequestration

Sequestration is a rare anomaly of the tracheobronchial tree. It has an estimated incidence of 0.15–1.7% in the general population. Sequestrations are classified as intralobar or extralobar. The nonfunctioning lung tissue lacks communication with the tracheobronchial tree and receives its supply from the arterial circulation. Intralobar sequestrations are the most common. The blood supply usually comes from the descending thoracic aorta, but in about 20% of cases, it comes from the upper abdominal aorta, celiac artery, or splenic artery. All pulmonary sequestrations should be treated surgically/interventionally because the high blood flow through the lesion can cause heart failure. Surgical procedures include ligation of the afferent vessels and/or resection of the pulmonary malformation.

In pulmonary sequestrations CT is superior to most other techniques, providing excellent information on both the vessels supporting the malformation (arterial and venous) and the structure of the lung parenchyma inside the malformation (**Fig. 23.8**). The spatial resolution of MR angiography may be too low to achieve adequate visualization of all vascular structures. Also, visualization of the lung parenchyma is difficult using MRI.

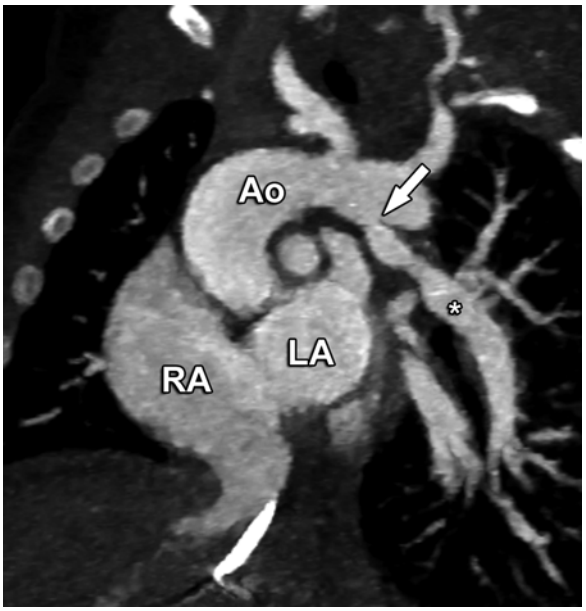

Fig. 23.9 Pulmonary artery arising anomalously from the aorta in a 2-day-old infant. This prospectively ECG-triggered high-pitch CT scan was performed without sedation and with an acquisition time of 0.25 s, 6 ml of contrast agent through a 24-G IV line, and a dose-length product of 5 Gy.cm. The image shows discontinuous pulmonary arteries, with the left pulmonary artery (*asterisk*) arising from the undersurface of the aortic arch (*Ao*, *arrow*). The patient underwent successful reimplantation of the branch pulmonary artery into the main pulmonary artery. *LA* left atrium, *RA* right atrium

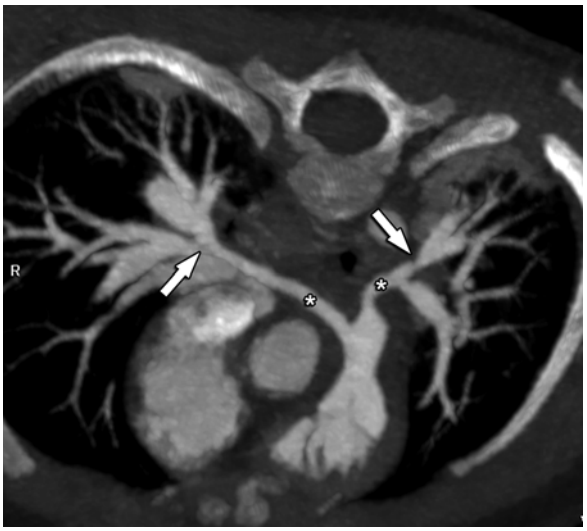

Fig. 23.10 Pulmonary branch hypoplasia in a 5-year-old patient with Williams syndrome. The 5-mm maximum intensity projection shows diffuse proximal branch pulmonary artery hypoplasia (*asterisks*) and focal distal pulmonary arterial narrowing (*arrows*). Because of the diffuse nature of the hypoplasia, no intervention was performed

23.5 Pulmonary Artery Pathology

Echocardiography is excellent for definition of the pulmonary valve and proximal pulmonary arteries, but is inadequate for distal pulmonary artery evaluation. CTA is well suited for detection of an absent pulmonary artery, a pulmonary artery arising anomalously from the aorta (**Fig. 23.9**) or aortopulmonary collateral arteries, and peripheral stenosis associated with certain genetic syndromes (**Fig. 23.10**) and for visualization of both the aortic and pulmonary arterial portions of the ductus arteriosus.

23.5.1 Origin of the Left Pulmonary Artery from the Right Pulmonary Artery (LPA Sling)

The left pulmonary artery arises aberrantly from the right pulmonary artery and runs between the trachea and esophagus to the left side, which either leads to an acute and severe airway compression (infants) or signs of chronic obstructive lung disease (childhood and young adults). Echocardiography is feasible in infants but further visualization of the airways is mandatory. CT is the recommended technique for visualization of the pulmonary arteries and the tracheobronchial tree (**Fig. 23.11**). Surgical correction is always performed with attachment of the left pulmonary artery to the pulmonary trunk anterior to the aorta.

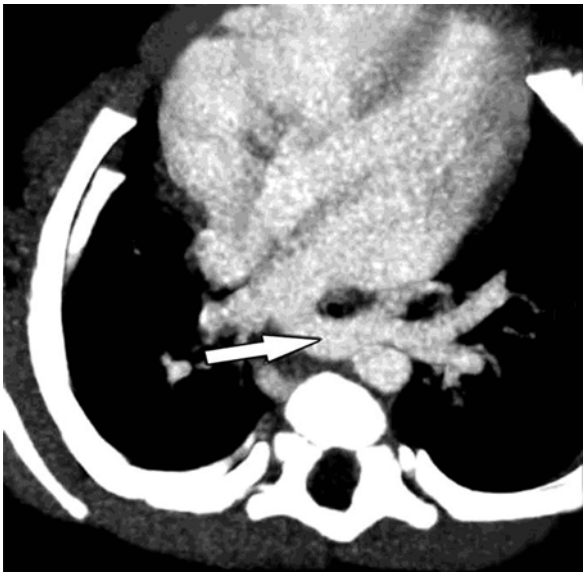

Fig. 23.11 Sling left pulmonary artery in a 5-month-old boy with a history of lower airway obstruction. Maximum intensity projection in the axial plane demonstrates a sling left pulmonary artery (*arrow*) that arises from the right pulmonary artery and courses posterior to the left main bronchus to supply the left lung. The child underwent reimplantation of the sling left pulmonary artery into the main pulmonary artery anterior to the trachea, relieving compression on the left main bronchus (With permission from A.-M. du Plessis et al. *Pediatr Radiol* 2008)

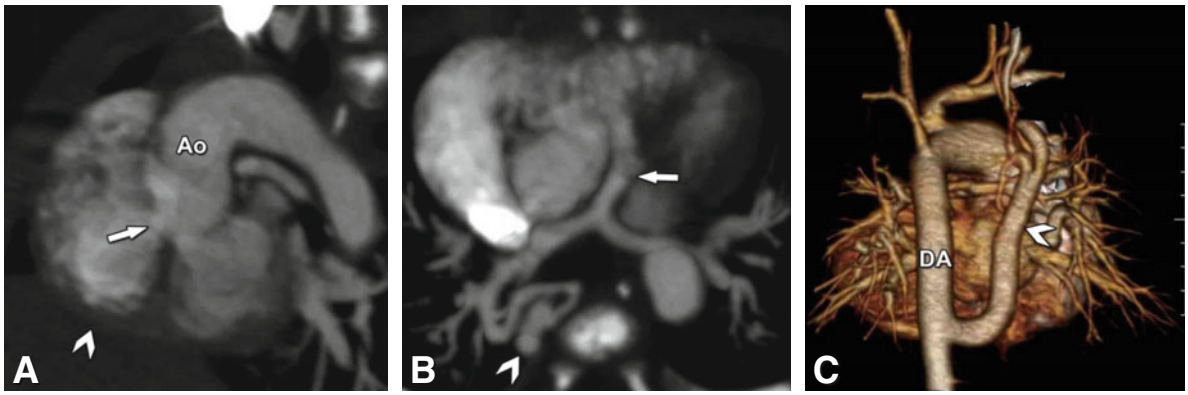

Fig. 23.12 Tetralogy of Fallot in a 1-month-old male baby. ECG-gated 16-row CT was performed using 30 ml of contrast agent with 250 mg I/ml followed by 10 ml saline at an injection rate of 1 ml/s through a venous line at the head. A larger amount of contrast agent was used to opacify the pulmonary arteries as well as the descending aorta and potential collaterals. **Panel A** (double-oblique reformation) shows the ventricular septal defect (*arrow*), the overstriding ascending aorta (*Ao*), and the right ventricular hypertrophy (*arrowhead*). **Panel B** (axial maximum intensity projection) shows the hypoplastic main (*arrow*), right and left pulmonary arteries and a large major aortopulmonary collateral artery (*MAPCA*) draining into the pulmonary arteries (*arrowhead*). The volume rendering (**Panel C**) shows the descending aorta (*DA*) and the large *MAPCA* (*arrowhead*), which is directed upwards. In this case the MAPCAs were too large for embolization and had to be clipped surgically

23.5.2 Tetralogy of Fallot

Tetralogy of Fallot (5–7% of CHD) is the most common right-sided obstructive anomaly. All forms of tetralogy include a large ventricular septal defect and varying degrees of obstruction to pulmonary outflow (**Fig. 23.12**), right ventricular hypertrophy, and aortic override of the ventricular septum. Surgical palliation includes septal defect closure and relief of the right ventricular outflow tract obstruction with a valvotomy, a patch, or a conduit from the right ventricle to the branch pulmonary arteries.

In tetralogy of Fallot with pulmonary artery atresia, lung perfusion is partly or completely provided by collaterals arising from the aortic arch. Defining the architecture of the central pulmonary arteries and aortopulmonary collaterals is essential for determining if the patient is suitable for primary correction. In patients with very small true pulmonary arteries and multiple aortopulmonary collateral vessels, a palliative shunt with unifocalization of the collaterals and pulmonary arteries is typically performed prior to complete repair. Subsequent corrective or palliative operations are usually possible, depending on the growth of the pulmonary arteries. The first aortopulmonary shunt described was the Blalock-Taussig shunt, connecting the subclavian artery to the ipsilateral pulmonary artery in cyanotic patients with tetralogy of Fallot (1944). Modified Blalock-Taussig shunts, central aortopulmonary shunts (using Goretex®), and direct connections of the hypoplastic pulmonary trunk to the aorta are in use today (**Fig. 23.12**). CT has been shown to correlate well with catheterization for evaluation of aortopulmonary collateral anatomy in patients with pulmonary artery atresia (**Fig. 23.12C**).

After complete repair of tetralogy, residual pulmonary stenosis and insufficiency are common and have a detrimental long-term effect on right ventricular function. Reintervention should be timed by evaluation of right ventricular end diastolic volume, end systolic volume, and right ventricular function. This data is most commonly obtained with MRI, but can be obtained with a functional CT dataset in patients with pacemakers or metal artifacts.

The incidence of additional coronary arterial anomalies in patients with tetralogy of Fallot is between 8 and 36%. The following anomalies in the course and/or distribution of the coronary arteries have been described: single coronary ostium, left anterior descending artery arising from the right coronary artery, circumflex artery arising from the right coronary artery, small fistulas between coronary arteries and the pulmonary artery, fistulas between coronary and bronchial arteries or right atrium. For CT in children with tetralogy of Fallot, a high diagnostic accuracy of 95.5% for all disease-related issues (compared to surgical findings) was found in a pilot study. Coronary artery anomalies are significant if they cross the right ventricular outflow tract and affect the planned surgical intervention.

In patients with a previously placed right ventricular outflow tract conduit or stent, CTA can be used to define the dimensions of the proximal and distal conduit, the branch pulmonary arteries, the in-stent luminal dimension, and the coronary artery relationship to the right ventricular outflow tract (**Figs.** 23.13, 23.14, and 23.15).

Fig. 23.13 Status post implantation of a pulmonary valve conduit (*arrows*) in a 2-year-old boy with tetralogy of Fallot (**Panel A**). **Panel B** shows the position of the ascending aorta (*Ao*) overstriding the large ventricular septal defect (*arrow*) between the right and left ventricle (*LV*). The examination was indicated to evaluate the anastomosis of the conduit to the native pulmonary arteries (*arrow* and *arrowhead* in **Panel C**). A focal stenosis of the lower lobe pulmonary artery (*arrowhead* in **Panel C**) can be seen. Interestingly, using MRI the spatial resolution was insufficient for precise visualization of the anastomoses, and interpretation was additionally impaired by artifacts from the mediastinal clips

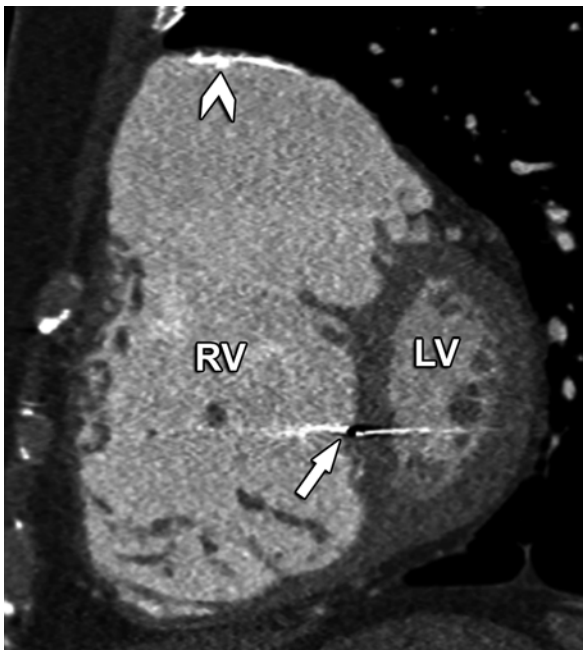

Fig. 23.14 This 30-year-old patient with repaired tetralogy of Fallot had severe pulmonary insufficiency and right ventricular enlargement. The scan was reconstructed in the short axis view from a functional CT scan. Note the transvenous pacer lead beam hardening artifact (*arrow*) and the calcified transannular patch (*arrowhead*). The patient underwent right ventricular outflow tract conduit placement. *LV* left ventricle, *RV* right ventricle

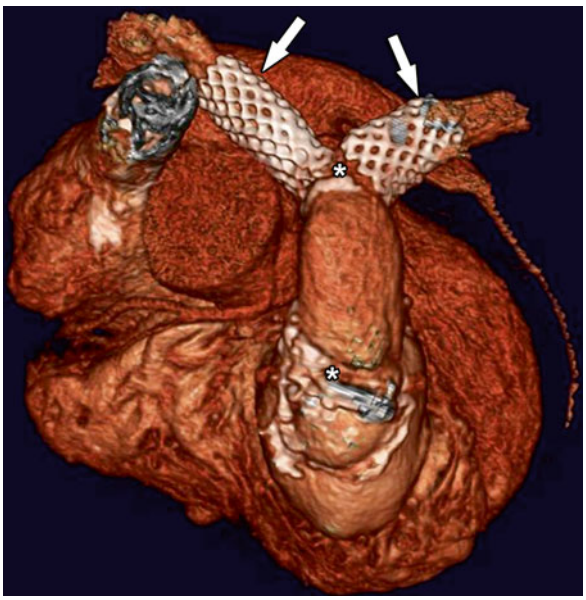

Fig. 23.15 This 20-year-old patient had a right ventricular outflow tract gradient on echocardiography, but the exact site of obstruction was unclear. A CT scan was performed because prior MR images were limited by artifacts. The three-dimensional reconstruction shows bilateral branch pulmonary artery stents (*arrows*) and extensive calcification of the proximal and distal conduit (*asterisks*). The pulmonary artery stents were patent (not shown). The patient underwent subsequent right ventricular outflow tract conduit placement

23.6 Left-Sided Heart Disease

Left-sided obstruction may occur at the level of the pulmonary veins, left atrium (cor triatriatum, Chap. 21), mitral valve, left ventricular outflow tract, or aortic arch (**List 23.2**). Patients may have obstruction at many levels and often have more than one lesion simultaneously. CT is excellent for visualization of total or partial anomalous pulmonary venous return (**Figs. 23.16** and **23.17**) and for complex arch anomalies, but most other lesions are seen very well echocardiographically. CTA is well suited to show the area of anatomic narrowing in cases of obstructed total or partial anomalous pulmonary venous return or the multiple sites of drainage in mixed anomalous pulmonary venous return. A small percentage of patients with obstructed total or partial anomalous pulmonary venous return will go on to develop pulmonary venous stenosis subsequent to repair, and the individual pulmonary vein, site and length of obstruction are well visualized by CTA.

Congenital anomalies of the aortic arch are common. Advanced imaging is usually requested for native arch pathology when there are associated cardiac anomalies or unusual features. CTA can detect aortic aneurysm, recurrent arch obstruction, or stent integrity and in-stent stenosis in patients who have undergone previous catheter-based or surgical intervention. CT can visualize the anatomy of an interrupted aortic arch, unusual ductus arteriosus, or truncus arteriosus to define aortopathy associated with Williams or Marfan syndrome.

List 23.2. Left-sided heart disease

1. Anomalous pulmonary venous return
   - Total anomalous pulmonary venous return (**Fig. 23.16**)
     - Cardiac
     - Infracardiac
     - Supracardiac
     - Mixed
   - Partial anomalous pulmonary venous return (often associated with atrial septal defects)
2. Pulmonary vein stenosis
3. Cortriatriatum (Chap. 21)
4. Aortic coarctation (**Figs. 23.3** and **23.4**)
   - Status post intervention (**Fig. 23.6**)
5. Interrupted aortic arch
6. Hypoplastic left heart syndrome
7. Aortopathy
   - Williams syndrome (**Fig. 23.10**)
   - Marfan syndrome

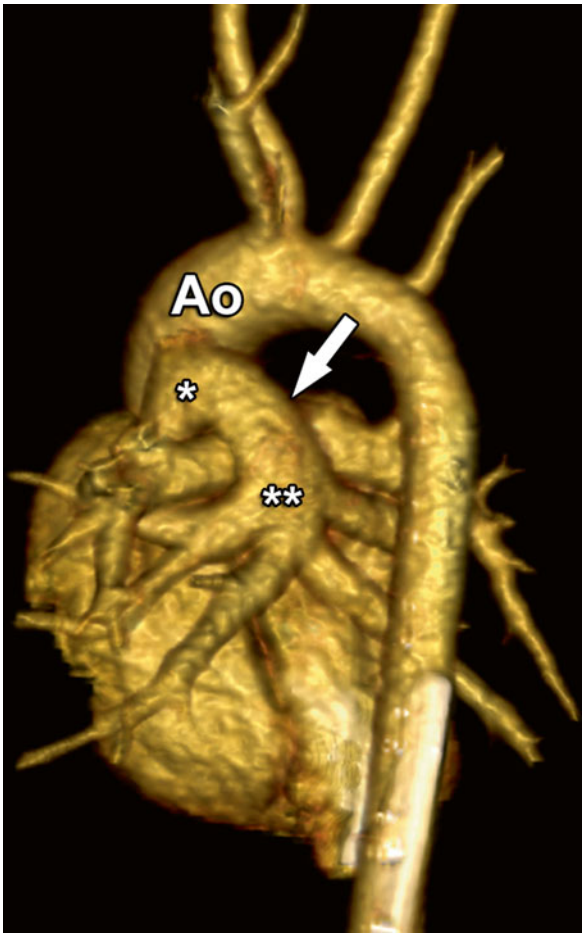

Fig. 23.16 This neonate presented with total anomalous pulmonary venous return (*TAPVR*) to the left superior vena cava (*asterisk*). A free-breathing CT scan was performed using 2 ml/kg of contrast agent injected through a 24-G IV line. The posterior view of a three-dimensional reconstruction shows the vertical vein (*arrow*) coursing over the left pulmonary artery and parallel to the aorta (*Ao*). The pulmonary venous confluence is indicated by two *asterisks*. The patient underwent TAPVR repair with connection of the pulmonary venous confluence to the left atrium

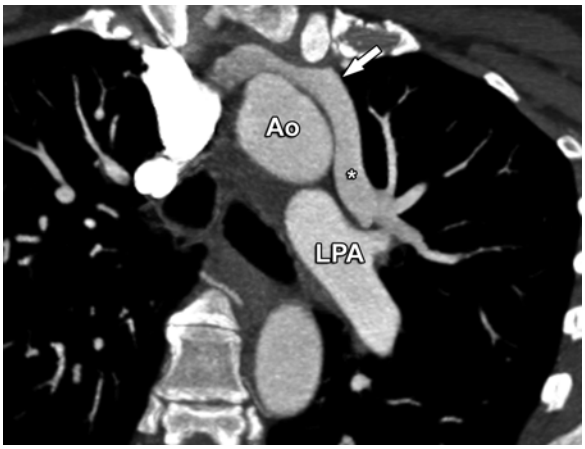

Fig. 23.17 Incidental finding of partial anomalous pulmonary venous return on a CT scan performed for coronary angiography. The axial maximum intensity projection shows the anomalous left upper pulmonary vein (*asterisk*) draining to the innominate vein (*arrow*). Due to the small shunt, no intervention was performed. *Ao* aorta, *LPA* left pulmonary artery

23.7 Transposition of the Great Arteries

Transposition of the great arteries (3–5% of newborn CHD) usually refers to isolated transposition of the great arteries (ventriculoarterial discordance, **Fig. 23.18**). Many older patients will have had an atrial switch, and younger patients will have undergone an arterial switch (**Fig. 23.19**). CTA easily visualizes the systemic and pulmonary venous baffles after atrial switch (**Figs. 23.18** and **23.19**) or the branch pulmonary arteries after the LeCompte maneuver (**Fig. 23.19C**), the reimplanted coronary arteries, and the neoaortic and neopulmonary root after the arterial switch. Although recent surgical outcomes are excellent, long-term follow-up for complications is required and repeat intervention is necessary in a minority of patients. Studies have shown that CTA correctly visualizes significant coronary lesions in these patients compared to catheterization angiography. L-TGA is also called physiologically corrected transposition and refers to both atrioventricular and ventriculoarterial

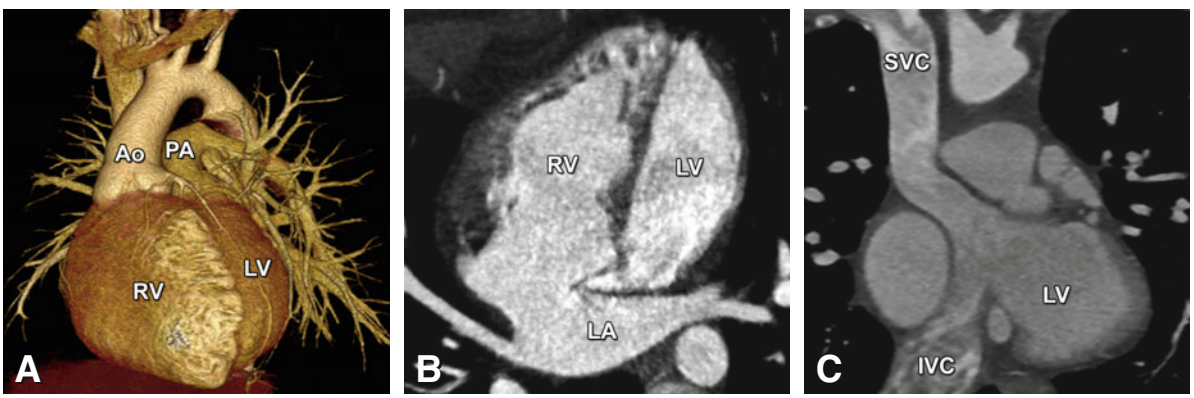

Fig. 23.18 A 27-year-old patient after atrial switch operation performed for transposition of the great arteries in the first year of life. CT images were acquired prospectively using high-pitch helical scanning. The three-dimensional reconstruction shown in **Panel A** illustrates d-transposition of the great arteries, with the anterior and rightward aorta (*Ao*) arising from the right ventricle (*RV*) and the leftward and posterior pulmonary artery (*PA*) arising from the normally positioned left ventricle (*LV*). Follow-up with echocardiography and possibly MRI will be required to screen for systemic right ventricular dysfunction, which is the most common reason for reduced life expectancy of patients with an atrial switch. **Panel B** shows the pulmonary venous baffle to the systemic right ventricle. This baffle is created at the time of the atrial switch to allow pulmonary venous blood to enter the right atrium and then fill the systemic right ventricle. **Panel C** is a coronal maximum intensity projection showing widely patent systemic venous baffles from the superior and inferior vena cava (*SVC* and *IVC*) to the *LV* after the atrial switch. Systemic venous baffle obstruction may occur in the future and is monitored by serial echocardiography or possibly MRI. It is important to assess baffle patency by opacification of the systematic venous system on CT in any patient with prior d-TGA and an atrial switch

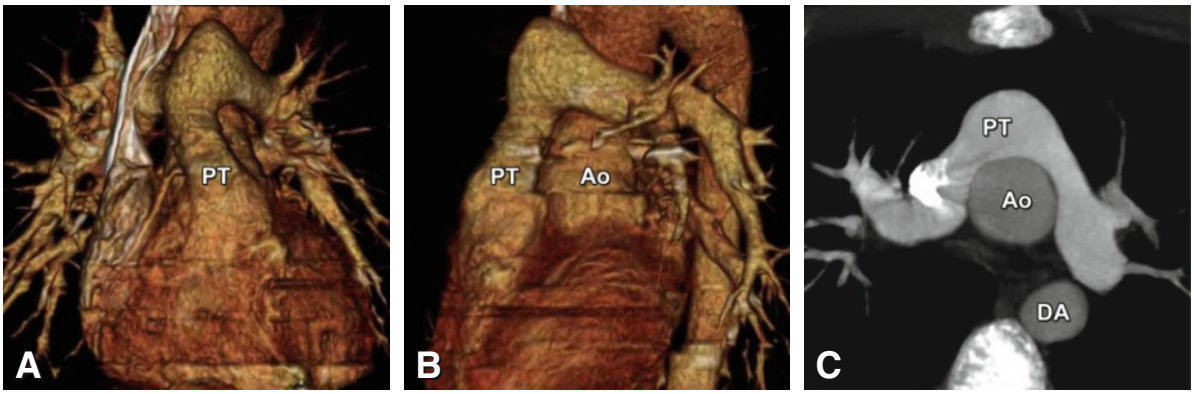

Fig. 23.19 Status post arterial switch operation for dextro-transposition of the great arteries in a 12-year-old boy. **Panels A** and **B** show three-dimensional volume renderings after surgery (anterior and lateral view, *PT* pulmonary trunk, *Ao* ascending aorta). No stenoses or aneurysms were found. An axial maximum intensity projection (**Panel C**) demonstrates the main pulmonary artery anterior to the ascending aorta (*Ao*), whereas there is a normal position of the descending aorta (*DA*)

discordance. Many of these patients have pacemakers due to the high incidence of congenital heart block.

Simultaneous visualization of both sides of the heart in transposition complexes can be accomplished with a biventricular injection protocol. CT of complex transposition must be tailored to the specific patient and operative details.

23.8 Coronary Artery Imaging

Coronary anomalies are classified according to their origin, course, and termination (**Figs.** 23.20 and 23.21). For further details on coronary anomalies pertaining to adults see Chap. 22. An abnormal coronary origin from the opposite sinus of Valsalva is the second most common cause of sudden death on the athletic field in the US. For anomalous left coronary arteries, the high risk interarterial course may be easily differentiated from the different benign courses. Treatment of an anomalous right coronary artery from the left-facing sinus remains a controversial topic.

23.8.1 Anomalous Origin of the Left Coronary Artery from the Pulmonary Artery (ALCAPA or Bland-White-Garland Syndrome)

The anomalous origin of the left coronary artery from the pulmonary artery (ALCAPA) is a rare congenital malformation reported to occur in 0.25–0.5% of all CHD. Most of the times, the anomaly is the only cardiac malformation. Less commonly, the association with other structural abnormalities may conceal the clinical findings and make the diagnosis even more difficult. Chronic myocardial ischemia leads to early progressive left heart failure and cardiac death. Children can survive if enough collaterals between the right coronary artery with a normal origin and the left coronary artery exist (formerly called adult type). This is only the case in 15–20% of patients. The other 80–85% patients do not have adequate collateral supply and develop progressive heart failure with death occurring at the age of 3–6 months. Usually, symptoms

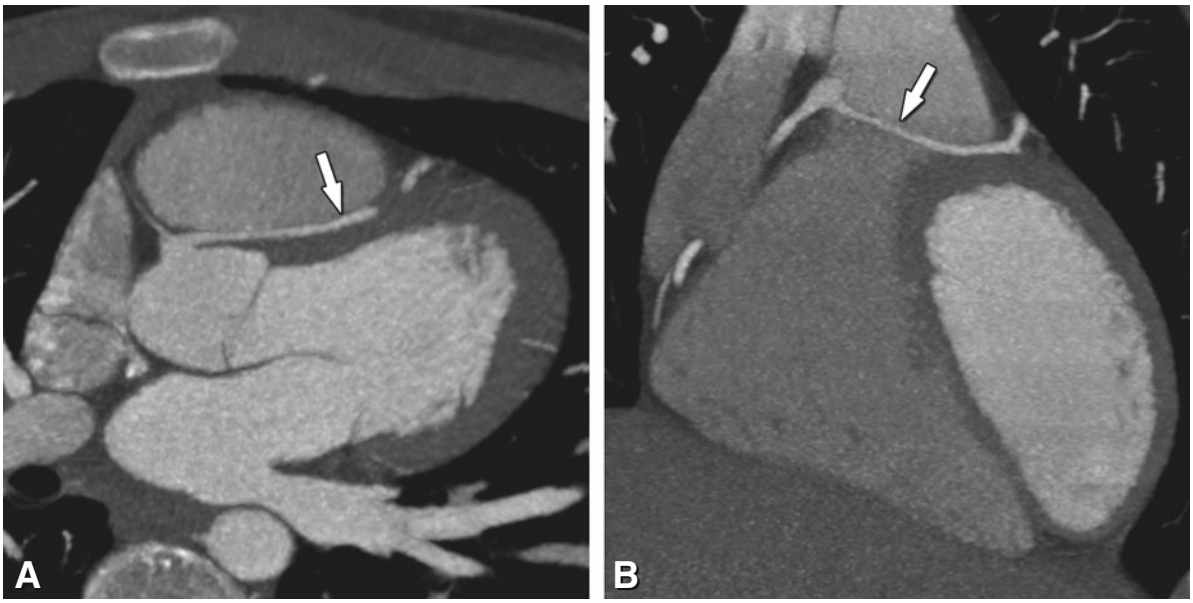

Fig. 23.20 Anomalous left coronary artery in a 10-year-old patient. The intraseptal benign course (Chap. 22) of an anomalous left coronary artery (*arrow*) from the right sinus of Valsalva is shown on maximum intensity projections in the axial (**Panel A**) and coronal orientation (**Panel B**). The course of the anomalous coronary artery is inferior to the pulmonary valve annulus through the septum. Although the patient presented with atypical chest pain, this anomaly is considered benign and unrelated to his symptoms

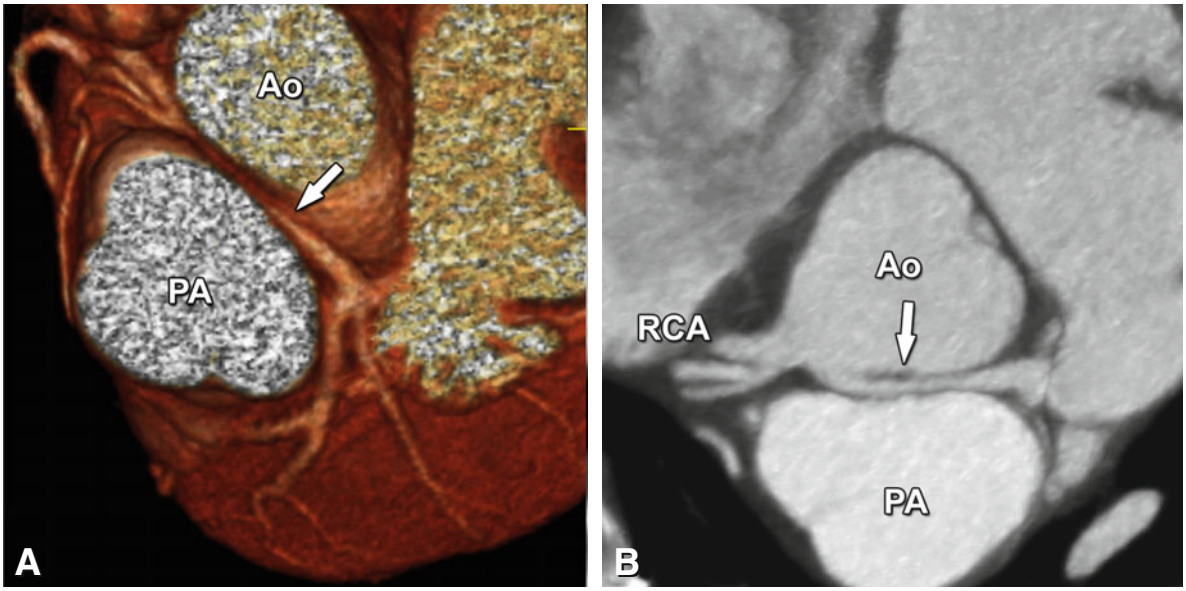

Fig. 23.21 Interarterial left coronary artery arising from the right sinus of Valsalva. This is a potentially malignant anomaly (*arrow*) with increased incidence of sudden death in those without surgical correction (**Panel A**). The maximum intensity projection (**Panel B**) demonstrates where surgical "unroofing" (*arrow*) will be performed to incorporate the left main coronary artery into the aortic sinus and eliminate coronary compression between the aorta (*Ao*) and pulmonary artery (*PA*). Surgical unroofing of the proximal course of the left coronary artery was performed and eliminated the patient's exertional chest pain. *RCA* right coronary artery

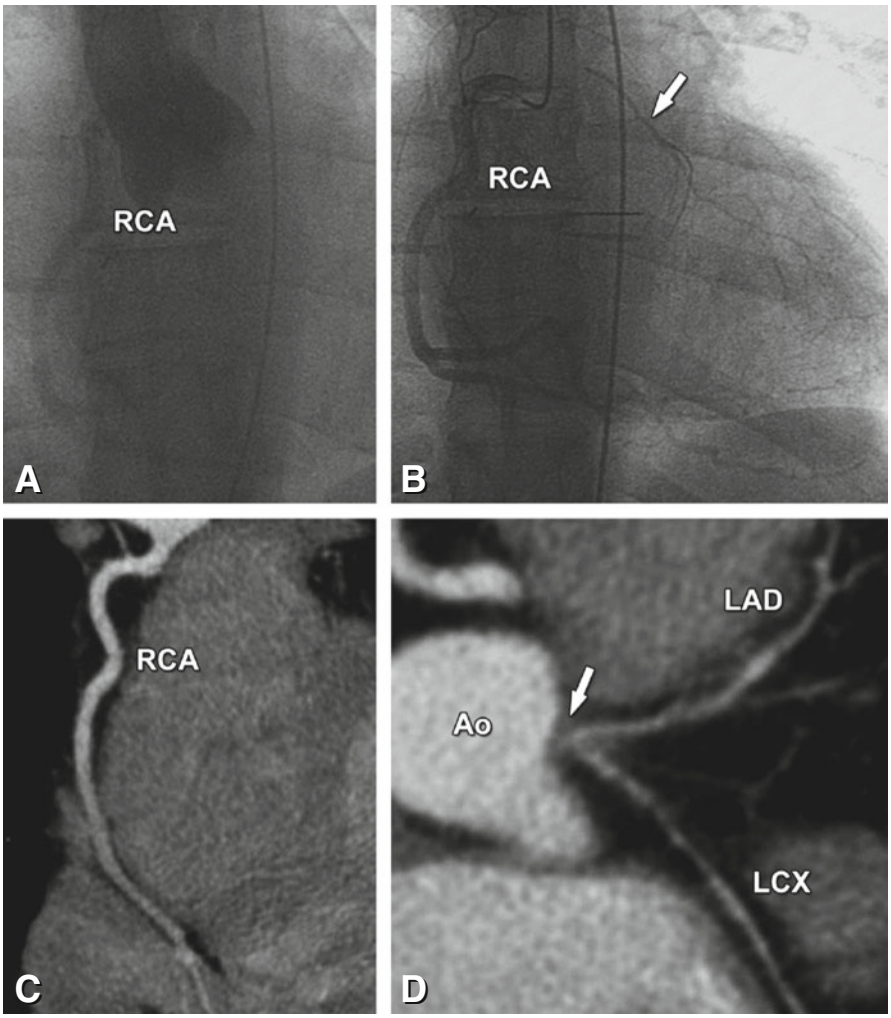

Fig. 23.22 Surgically corrected Bland-White-Garland syndrome in a 16-year-old girl. The left main coronary artery originated from the pulmonary artery and was surgically transferred to the aortic root during infancy to restore normal anatomy. Additionally, a mechanical mitral valve was placed. Conventional angiography (aortography) at follow-up demonstrated the right coronary artery (*RCA*, **Panel A**) but not the ostium of the left coronary artery. A late phase of the dedicated angiography of the *RCA* demonstrated retrograde filling of the left coronary arterial system (*arrow* in **Panel B**) as an indirect sign of left main occlusion. The patient had no clinical symptoms or ECG changes. 16-row CT using adaptive multisegment reconstruction ruled out stenosis of the dominant *RCA* (**Panel C**, curved multiplanar reformation) but also confirmed the occlusion of the reinserted left main coronary artery (*arrow* in **Panel D**, curved multiplanar reformation, *Ao* ascending aorta). Both the left anterior descending (*LAD*) and the left circumflex coronary artery (*LCX*) were opacified on CT due retrograde filling via collaterals from the *RCA*

present late, and the clinical examination is inconspicuous. If there is a clinical suspicion, at this point, CT can reliably detect the anomalous origin of the left coronary artery. It should be kept in mind that scanning should be started when the contrast agent is in the ascending aorta (as usual) as there is retrograde filling of the left coronary artery by the right coronary artery (**Fig. 23.22**).

Coronary artery stenosis is rare in childhood, but has been reported early and late after arterial switch operations, after reimplantation as part of the Ross procedure (a diseased aortic valve is replaced with the person's own pulmonary valve, a pulmonary allograft (valve taken from a cadaver) replaces the patient's own pulmonary valve), and in patients with a history of Kawasaki disease and aneurysms.

23.8.2 Kawasaki Disease

Kawasaki disease is an acute, self-limiting vasculitis of unknown etiology that occurs predominantly in infants and young children. It was first described in 1967 by Dr. Tomisaku Kawasaki in the Japanese literature (Arerugi). The specific cause of the disease is still unknown. Current theories center primarily on immunological causes. Classically, 5 days of fever plus four of five diagnostic criteria must be met to establish the diagnosis. By far the highest incidence of Kawasaki disease occurs in Japan (175 per 100,000 patients under 5 years of age), though its incidence in the US is increasing (approximately 2,000–4,000 cases are identified in the US each year). Kawasaki disease is predominantly a disease of young children, with 80% of patients being younger than 5 years of age. The disease affects more boys than girls.

Cardiac complications are the most important aspect of the disease. Kawasaki disease can cause vasculitis in the coronary arteries and subsequent coronary artery aneurysms. These aneurysms can lead to myocardial infarction even in young children (**Fig. 23.23**). Overall, about 5–20% of children with Kawasaki disease develop coronary artery aneurysms with much higher prevalence among patients who are not treated with intravenous immunoglobulins (IVIG) early in the course of illness (**Fig. 23.24**). Virtually all deaths in patients with Kawasaki disease result from its cardiac sequelae. Mortality peaks 15–45 days after the onset of fever; at this stage, patients have coronary vasculitis with a concomitant marked elevation of the platelet count and a hypercoagulable state. However, sudden death from myocardial infarction may also occur many years later in individuals who develop coronary stenoses following a childhood history of coronary artery aneurysms. Many cases of fatal and nonfatal myocardial infarction in young adults have been attributed to "missed" Kawasaki disease in childhood.

Evaluation of the coronary arteries should include quantitative assessment of internal vessel diameters (**Fig. 23.25**). Aneurysms are at least 1.5 times larger than the surrounding reference vessel diameter and are classified as saccular if axial and lateral diameters are nearly equal or as fusiform if symmetric dilatation with gradual proximal and distal tapering is seen. When a coronary artery is larger than normal without a segmental aneurysm, the vessel is considered ectatic. Standard deviations (called Z-scores) are commonly used to determine if the coronary artery is dilated relative to the patient's body surface area. Care must be taken in making the diagnosis of ectasia because of considerable normal variation in coronary artery distribution and dominance. The Japanese Ministry of Health criteria classify coronary arteries as abnormal (ectatic) if the internal lumen diameter is >3 mm in children <5 years of age or >4 mm in children ≥5 years of age, if the internal diameter of a segment measures ≥1.5 times that of an adjacent segment, or if the coronary lumen is clearly irregular. This is less commonly

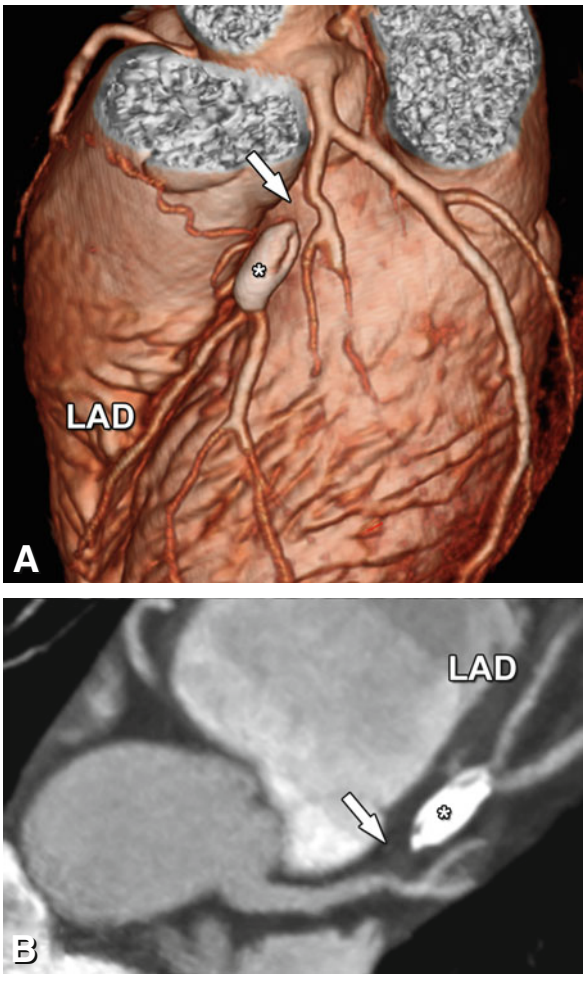

Fig. 23.23 Routine follow-up CT performed in 24-year-old patient who had severe Kawasaki disease at a young age. The three-dimensional reconstruction (**Panel A**) and maximum intensity projection (**Panel B**) show complete occlusion (*arrow*) of the left anterior descending coronary artery (*LAD*) proximal to a calcified aneurysm (*asterisk*). The patient is now managed medically by an adult cardiologist

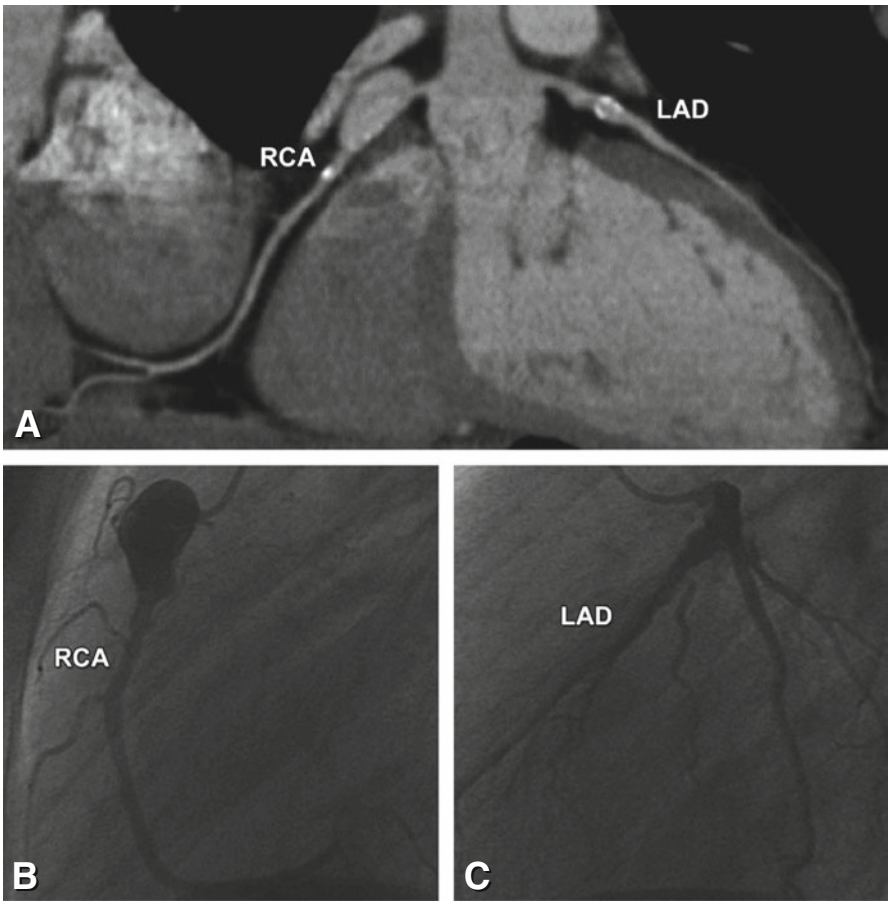

Fig. 23.24 A 25-year-old male patient with Kawasaki disease. The disease occurred at the age of 2 and resulted in a giant aneurysm of the proximal right coronary artery (*RCA*) and a fusiform aneurysm in the left anterior descending coronary artery (*LAD*) seen at CT follow-up (curved multiplanar reformation, **Panel A**). Conventional coronary angiography confirmed these findings in the *RCA* (**Panel B**) and LAD (**Panel C**). The RCA aneurysm was 25 mm long and had a diameter of 12.5 mm on CT (Used with permission from Arnold et al. *Pediatr Radiol* 2007)

Fig. 23.25 A 21-year-old patient with Kawasaki disease and aneurysms of both the left anterior descending coronary artery (*LAD*, **Panels A**–**D**) and the right coronary artery (*RCA*, **Panels E** and **F**). The LAD aneurysm was severely calcified (**Panel B**, curved multiplanar reformation), and stenosis was demonstrated distal to the aneurysm (*arrow* in **Panels A** and **D**). However, the percent diameter stenosis was difficult to evaluate using CT due to the aneurysmal calcification (**Panel D**). There was no stenosis and aneurysm in the left circumflex coronary artery (*LCX*) both on conventional coronary angiography (**Panel A**) and prospectively ECG-gated dual-source CT (**Panel C**). There was no significant stenosis in the *RCA* as seen on conventional coronary angiography (**Panel E**). The CT examination was superior in visualizing the calcifications in the aneurysm and also did not show any stenosis (**Panel F**). However, there was an artifact on CT as seen in **Panels C**, **D**, and **F** (*asterisks*), which was due to arrhythmia

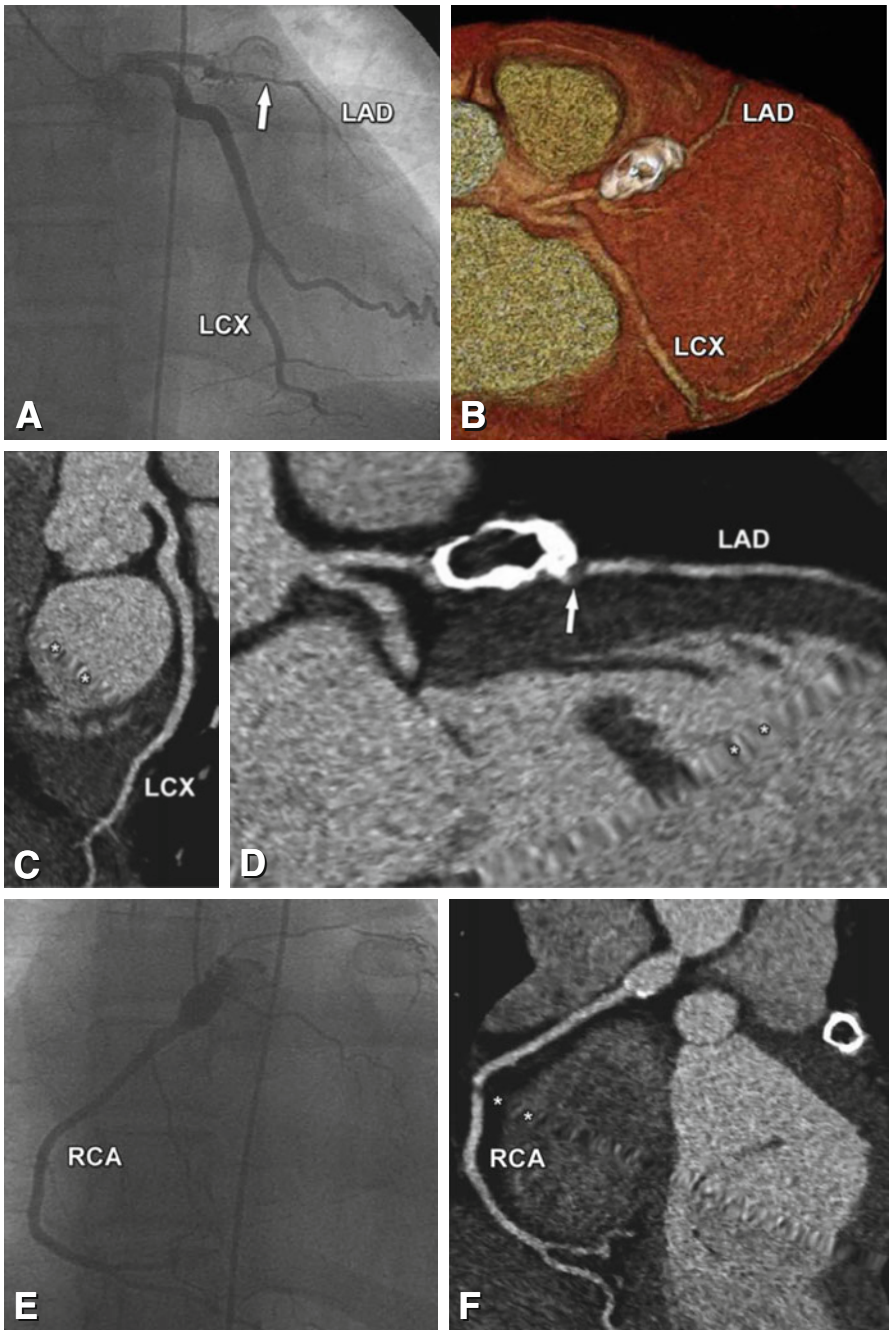
LAD
LCX
A
LAD
LCX
B
LCX
C
LAD
D
RCA
E
RCA
F

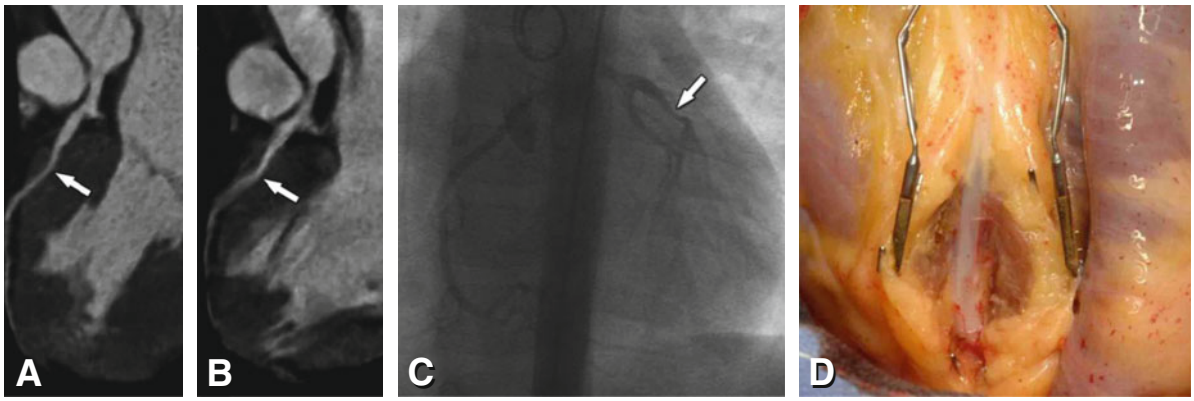

Fig. 23.26 An 11-year-old girl with myocardial bridging of the left anterior descending coronary artery (*LAD*) due to hypertrophic cardiomyopathy. She was admitted to the hospital after a heart attack and resuscitation and was thus referred for CT, which was performed on a dual-source CT scanner at a heart rate of 103 beats per min. The patient showed only limited breath-hold capabilities, leading to artifacts on the reconstructed images. ECG-gated CT angiography using 50 ml of an iodinated contrast agent (370 mg iodine/ml) shows the intramural segment (*arrows*) of the left anterior descending coronary artery displayed as curved multiplanar reformations during systole (**Panel A**) and diastole (**Panel B**). Note the narrow lumen (*arrow*) of the intramural segment during systole and diastole (**Panels A** and **B**). This finding was confirmed on conventional angiography (*arrow* in **Panel C**). **Panel D** shows the intraoperative site after dissection of the myocardium. The further clinical course was uneventful (**Panel D** is courtesy of Dr. C. Sebening, Heidelberg)

used now that the Z-score standard deviations are widely available.

Proximal aneurysm can be evaluated echocardiographically, but the technique is not sensitive enough to exclude coronary stenosis. For evaluation of stenosis or of the more distal coronary segments, either conventional coronary angiography or CT is required. Small studies in follow-up patients (mostly teenagers) have confirmed an almost 100% diagnostic accuracy of CT for detection of aneurysms with conventional coronary angiography as the reference standard. Thus, recent CT scanners can be recommended for noninvasive follow-up after childhood Kawasaki disease, while severe calcifications may still impair estimates of the degree of coronary stenosis.

23.8.3 Myocardial Bridging

Normally, coronary arteries have an epicardial course. A myocardial bridge is a congenital condition in which a segment of coronary artery runs intramurally, through the myocardium, beneath a muscular bridge. The coronary artery segment covered by the myocardial bridge is called a "tunneled" artery. As the heart contracts to pump blood, the muscle exerts pressure across the bridge and may constrict the artery. This can lead to premature ventricular contractions and angina pectoris. There are only case reports on the use of CT for diagnosing myocardial bridging in children. Bridging is most commonly seen in children with hypertrophic cardiomyopathy.

Myocardial bridging most often affects the left anterior descending coronary artery. Mild forms of myocardial bridging (less than 20% diameter stenosis) are often undetectable, as the blood usually flows through the coronary while the heart is relaxing in diastole. Visualization of the coronary arteries during diastole and systole is mandatory to determine the percentage of diameter stenosis and measure the lengths of the tunneled part for planning the surgical strategy in patients with ischemia (**Fig. 23.26**). The effect of myocardial bridging is very controversial and many think it is a normal variant that does not require intervention.

Fig. 23.27 Paravalvular leak after prosthetic mitral valve implantation (*arrow*). This adult patient had undergone multiple prior prosthetic mitral valve placements for her partial atriventricular canal and cleft mitral valve. Approximately 1 year after her last valve replacement, she was found to have an increasing mitral gradient. A functional CT scan was performed for evaluation of left ventricular volumes and regurgitant fraction. A four-chamber view shows a large paravalvular leak of the lateral mitral valve annulus. The severity of insufficiency had been underestimated by transesophageal echocardiography, and increased flow wrongly suggested mitral stenosis with an increased gradient. The valve was subsequently replaced and the patient markedly improved

23.9 Evaluation of Prosthetic Valves

Pediatric patients often have a mechanical (**Fig. 23.13**a) or bioprosthetic valve (**Fig. 23.27**) placed as part of complex palliation. There is an expected gradient through any prosthetic valve, but the gradient can increase due to valve dysfunction, patient-valve size mismatch with somatic growth, or pannus formation. Perivalvar leaks are also seen, and they are difficult to quantify or see by echocardiography due to the artifact from the valve structure itself. CTA is an excellent modality to assess bioprosthetic valve function, pannus formation, and paravalvular leaks (**Fig. 23.27**, Chaps. 16, 17, and 18). For leaks, the regurgitant fraction can be calculated from a function scan based on the stroke volume differences between the right and left ventricle.

Recommended Reading

Angeli E, Formigari R, Pace Napoleone C, Oppido G, Ragni L, Picchio FM et al (2010) Long-term coronary artery outcome after arterial switch operation for transposition of the great arteries. Eur J Cardiothorac Surg 38:714–720

Arnold R, Ley S, Ley-Zaporozhan J et al (2007) Visualization of coronary arteries in patients after childhood Kawasaki syndrome: value of multidetector CT and MR imaging in comparison to conventional coronary catheterization. Pediatr Radiol 37:998–1006

Bland EF, White PD, Garland J (1933) Congenital anomalies of the coronary arteries: report of an unusual case associated with cardiac hypertrophy. Am Heart J 8:787–801

Burns JC, Glode MP (2004) Kawasaki syndrome. Lancet 364:533–544

Daebritz SH, Nollert G, Sachweh JS, Engelhardt W, von Bernuth G, Messmer BJ (2000) Anatomical risk factors for mortality and cardiac morbidity after arterial switch operation. Ann Thorac Surg 69:1880–1886

Ferguson EC, Krishnamurthy R, Oldham SA (2007) Classic imaging signs of congenital cardiovascular abnormalities. Radiographics 27:1323–1334

Frush DP, Siegel MJ, Bisset GS 3rd (1997) From the RSNA refresher courses. Challenges of pediatric spiral CT. Radiographics 17:939–959

Han BK, Lindberg J, Grant K, Schwartz RS, Lesser JR (2011) Accuracy and safety of high pitch computed tomography imaging in young children with complex congenital heart disease. Am J Cardiol 107:1541–1546

Haramati LB, Glickstein JS, Issenberg HJ, Haramati N, Crooke GA (2002) MR imaging and CT of vascular anomalies and connections in patients with congenital heart disease: significance in surgical planning. Radiographics 22:337–347, discussion 48–9

Hayabuchi Y, Inoue M, Watanabe N, Sakata M, Nabo MM, Kitagawa T et al (2010) Assessment of systemic-pulmonary collateral arteries in children with cyanotic congenital heart disease using multidetector-row computed tomography: comparison with conventional angiography. Int J Cardiol 138:266–271

Hoffmann A, Engelfriet P, Mulder B (2007) Radiation exposure during follow-up of adults with congenital heart disease. Int J Cardiol 118:151–153

Hughes D Jr, Siegel MJ (2010) Computed tomography of adult congenital heart disease. Radiol Clin North Am 48:817–835

Jacobs JP, Mavroudis C, Jacobs ML, Maruszewski B, Tchervenkov CI, Lacour-Gayet FG et al (2007) Nomenclature and databases – the past, the present, and the future : a primer for the congenital heart surgeon. Pediatr Cardiol 28:105–115

Jatene AD, Fontes VF, Paulista PP et al (1976) Anatomic correction of transposition of the great vessels. J Thorac Cardiovasc Surg 72:364–370

Konstantinov IE, Alexi-Meskishvili VV, Williams WG, Freedom RM, Van Praagh R (2004) Atrial switch operation: past, present, and future. Ann Thorac Surg 77:2250–2258

Lell MM, May M, Deak P, Alibek S, Kuefner M, Kuettner A et al (2011) High-pitch spiral computed tomography: effect on image quality and radiation dose in pediatric chest computed tomography. Invest Radiol 46:116–123

Ley S, Zaporozhan J, Arnold R et al (2007) Preoperative assessment and follow-up of congenital abnormalities of the pulmonary arteries using CT and MRI. Eur Radiol 17:151–162

Lin MT, Wang JK, Chen YS, Lee WJ, Chiu HH, Chen CA et al (2012) Detection of pulmonary arterial morphology in tetralogy of Fallot with pulmonary atresia by computed tomography: 12 years of experience. Eur J Pediatr 171:579–586

Oh KH, Choo KS, Lim SJ, Lee HD, Park JA, Jo MJ et al (2009) Multidetector CT evaluation of total anomalous pulmonary venous connections: comparison with echocardiography. Pediatr Radiol 39:950–954

Ou P, Celermajer DS, Marini D et al (2008) Safety and accuracy of 64-slice computed tomography coronary angiography in children after the arterial switch operation for transposition of the great arteries. JACC Cardiovasc Imaging 1:331–339

Paul JF, Rohnean A, Elfassy E, Sigal-Cinqualbre A (2011) Radiation dose for thoracic and coronary step-and-shoot CT using a 128-slice dual-source machine in infants and small children with congenital heart disease. Pediatr Radiol 41:244–249

Prakash A, Powell AJ, Geva T (2010) Multimodality noninvasive imaging for assessment of congenital heart disease. Circ Cardiovasc Imaging 3:112–125

Rigsby CK, Gasber E, Seshadri R, Sullivan C, Wyers M, Ben-Ami T (2007) Safety and efficacy of pressure-limited power injection of iodinated contrast medium through central lines in children. AJR Am J Roentgenol 188:726–732

Trowitzsch E, Berger T, Stute M (1991) The diameter of the large arteries in the first 3 years of life. An echocardiography study. Monatsschr Kinderheilkd 139:355–359

Vastel-Amzallag C, Le Bret E, Paul JF, Lambert V, Rohnean A, El Fassy E et al (2011) Diagnostic accuracy of dual-source multislice computed tomographic analysis for the preoperative detection of coronary artery anomalies in 100 patients with tetralogy of Fallot. J Thorac Cardiovasc Surg 142:120–126

Vyas HV, Greenberg SB, Krishnamurthy R (2012) MR imaging and CT evaluation of congenital pulmonary vein abnormalities in neonates and infants. Radiographics 32:87–98

Walhout RJ, Suttorp MJ, Mackaij GJ, Ernst JM, Plokker HW (2009) Long-term outcome after balloon angioplasty of coarctation of the aorta in adolescents and adults: is aneurysm formation an issue? Catheter Cardiovasc Interv 73:549–556

Warnes CA (2006) Transposition of the great arteries. Circulation 114:2699–2709

Warnes CA, Williams RG, Bashore TM, Child JS, Connolly HM, Dearani JA et al (2008) ACC/AHA 2008 guidelines for the management of adults with congenital heart disease: a report of the American College of Cardiology/American Heart Association Task Force on practice guidelines (writing committee to develop guidelines on the management of adults with congenital heart disease). Circulation 118:714–833